# RPC-LAP Science Data User Guide

RO-IRFU-LAP-UG
Version 1.2.2
December 10, 2020

Anders Eriksson and Fredrik Leffe Johansson

**Document history**

| Version | Date | Sections changed | Notes |
|---|---|---|---|
| 1.0 | 2019-03-31 | New document. | Initial revision. |
| 1.1 | 2019-07-12 | | Revised after peer review, with addition of material for data set versions delivered July 2019. |
| 1.2 | 2019-09-23 | 5.1 (Figs 1 & 2) 5.8 (Fig 8) All (editorial) | Update of Fig 1 to latest version in archive. Corrected angle definition in Fig 2. Corrected unit of frequency in Fig 8. Minor editorial changes and corrections. |
| 1.2.1 | 2020-01-20 | | Mostly editorial changes |
| 1.2.2 | 2020-12-10 | | Changed "plasma density" to "electron density" |

# Contents

# 1  Scope

This user guide is intended as a practical introduction for typical science users of the data from the LAngmuir Probe instrument (LAP) of the Rosetta Plasma Consortium (RPC) archived in the ESA Planetary Science Archive. Technical details on the instrument and the archive are treated in depth in the [EAICD]. An overall introduction to all RPC data, including LAP, can be found in the [RPC User Guide].

# 2  Brief introduction

The ESA Rosetta mission to comet 67P/Churyumov-Gerasimenko carried a small but comprehensive set of plasma instruments known as the Rosetta Plasma Consortium (RPC), monitoring the cometary plasma from arrival in August 2014 to end of mission in September 2016. Among the RPC instruments was the Langmuir probe instrument LAP, with chief mission to measure:

- Electron density, ne
- Spacecraft potential, Vsc
- Electron temperature, Te
- Electric field, E
- Ion flow speed, ui
- Photoemission current, Iph
- Wave activity

The LAP sensors are two spherical probes, 5 cm in diameter, known as LAP1 and LAP2, one on each of the two booms protruding a few meters from the s/c body (**Figure 2**). The primary parameter actually measured by the instrument is the current flowing to (or the voltage of) a probe when some bias voltage (or bias current) is applied to it, which is the data transmitted to ground. From these data the parameters above have been derived, for some products also with use of data from RPC-MIP. Do not expect all parameters to be available at any given time.

# 3  Conventions

The detailed format of the LAP data files in ESA's planetary science archive is discussed in the LAP EAICD. For the purposes of this User Guide, it is convenient to refer to specific data products available in these files as, for example, "the U_SC parameter in the USC files". Here U_SC is the name of the data product as given in the label (.LBL) files attached to each data (.TAB) file, while "USC file" is to be understood as a data (.TAB) file containing the string "USC" in its file name.

As an example, consider the contents of the directory containing Level 5 DERIV2 (see Section 4 below for archive levels) data from Feb 10, 2016:

```
LAP_20160210_000000_60M_PHO.LBL    LAP_20160210_000414_PSD_I1H.TAB
LAP_20160210_000000_60M_PHO.TAB    LAP_20160210_000414_PSD_I2H.LBL
LAP_20160210_000000_BLKLIST.LBL    LAP_20160210_000414_PSD_I2H.TAB
LAP_20160210_000000_BLKLIST.TAB    LAP_20160210_120206_32S_V1D.LBL
LAP_20160210_000000_GEOM.LBL       LAP_20160210_120206_32S_V1D.TAB
LAP_20160210_000000_GEOM.TAB       LAP_20160210_120206_32S_V2D.LBL
LAP_20160210_000414_32S_I1D.LBL    LAP_20160210_120206_32S_V2D.TAB
LAP_20160210_000414_32S_I1D.TAB    LAP_20160210_120206_802_EFL.LBL
LAP_20160210_000414_32S_I2D.LBL    LAP_20160210_120206_802_EFL.TAB
LAP_20160210_000414_32S_I2D.TAB    LAP_20160210_120206_802_NPL.LBL
LAP_20160210_000414_914_ASW.LBL    LAP_20160210_120206_802_NPL.TAB
LAP_20160210_000414_914_ASW.TAB    LAP_20160210_120206_802_USC.LBL
LAP_20160210_000414_914_NPL.LBL    LAP_20160210_120206_802_USC.TAB
LAP_20160210_000414_914_NPL.TAB    LAP_20160210_120206_FRQ_V1H.LBL
LAP_20160210_000414_914_USC.LBL    LAP_20160210_120206_FRQ_V1H.TAB
LAP_20160210_000414_914_USC.TAB    LAP_20160210_120206_FRQ_V2H.LBL
LAP_20160210_000414_FRQ_I1H.LBL    LAP_20160210_120206_FRQ_V2H.TAB
LAP_20160210_000414_FRQ_I1H.TAB    LAP_20160210_120206_PSD_V1H.LBL
LAP_20160210_000414_FRQ_I2H.LBL    LAP_20160210_120206_PSD_V1H.TAB
LAP_20160210_000414_FRQ_I2H.TAB    LAP_20160210_120206_PSD_V2H.LBL
LAP_20160210_000414_PSD_I1H.LBL    LAP_20160210_120206_PSD_V2H.TAB
```

There are two "USC files" for this day, `LAP_20160210_000414_914_USC.TAB` and `LAP_20160210_120206_802_USC.TAB`. Two files of the same type (e.g. USC) never overlap, and the start time of each data file is indicated in its name, so the two USC files cover the first and second half of the day, respectively.

# 4  Data availability

All LAP data acquired at the comet are stored in and available from ESA's Planetary Science Archive (PSA), and also NASA's Planetary Data System (PDS). LAP data are archived at three levels of processing in four datasets:

- L2 (EDITED): Full time resolution time-tagged samples in raw telemetry units, no offsets removed, time not compensated for filter group delay. Contains all data produced by the instrument in space, except some small amounts of packets discarded for technical reasons.
- L3 (CALIBRATED): Full time resolution L2 data converted to instrument units (volts and ampères) with known offsets removed, time tags adjusted for filter group delay and onboard averaging. Coverage almost as complete as L2.
- L5 (DERIVED): The PI team's best values for electron density and temperature, spacecraft potential, electric field and effective ion speed, derived from the L3 data, often cross-calibrated with the Mutual Impedance Probe instrument (RPC-MIP). Some data at highest time resolution, but most files contain data with time resolution of 32 s or longer. Some products (e.g. low time resolution s/c potential proxy and electron density) cover almost all the mission while other are limited to particular

operational modes (e.g. electric field estimates) run a few per cent of the total time. L5 data is separated into two datasets:

  - ○ DERIV2, which contains all afore-mentioned science data parameters except one.
  - ○ NEL, which contains the highest time resolution cross-calibrated density data, when RPC-MIP is not delivering cross-calibrated density products.
- RPC-MIP archive: Full time resolution (often 16 ms, otherwise 0.55, 1.1 or 2.2 s) LAP currents and voltages calibrated to electron density by use of scarcer RPC-MIP data are delivered to the PSA by the MIP team and hence included in the MIP archive. Limited coverage as only possible to obtain when both MIP and LAP are in suitable modes and have good data quality.

The typical scientist will probably only need the data in the LAP L5 archive and/or the high-time resolution LAP-MIP electron density in the MIP archive. For some special scientific needs advanced users may wish also to use some L3 files. The L2 data are of possible interest only to users with very specific technical needs out of the scope of this guide.

The LAP L2 archive contains all data produced by the instrument in space, except some small amounts of packets discarded for technical reasons. Almost all the data can be calibrated to L3 and is then available in the L3 archive. The scientifically most useful data set, L5, does cover the full mission at the comet but is much smaller in volume as it has not been possible to calibrate all highest time resolution data to electron density in a consistent way, and as most of the highest quality LAP data actually is found in the MIP-LAP cross calibrated data delivered by RPC-MIP.

# 5  The LAP data

We assume you are interested in science data on any of the main LAP parameters. What to look for is discussed below for each of them. For an overview of all data products, the daily browse plots (example in **Figure *1***) are very useful and it is recommended to look at such plots when reading this document. We therefore start with describing the browse plots.

## 5.1  Browse plots

Daily LAP browse plots are available in the BROWSE directory of the LAP DERIV2 data sets. Each browse plot PNG image shows two pages as shown in the example in **Figure *1***. In this Section we describe the content of each panel, deferring discussion of the interpretation to the corresponding subsections below. The plots are intended to give a handy overview of LAP data and provide some context by also showing spacecraft position and pointing.

All browse plots have the same layout, and always cover one UTC calendar day (24 hours). If LAP science data are missing for some time interval, either completely or just some type of data not being available in some particular instrument mode, the corresponding part of that panel is blank. If there are no LAP science data at all for a full day, no browse plot is produced. There is a left and a right side in each plot, with the information at left generally being more "low level", directly illustrating data recorded by LAP, while the panels at right give the physical parameters derived from these.

Most panels in the browse plots are based on data from the LAP DERIV2 data set. However, two panels (panels (d) and (e) **Figure *1***) show data from the CALIB2 data set. When we in the following subsections tell which quantities are plotted and what files they originate from, they are all found in the DERIV2 data sets unless otherwise specified. We also plot geometry data, available in the LAP geometry files in the CALIB2 and DERIV2 data sets.

As described in the EAICD, LAP operational modes are controlled by "macros", small repeated sequences uploaded to the instrument defining all aspects of how LAP runs. This is mostly a technical detail, but to have comparable data users may for example be interested in looking for data for some particular macro. One run of a particular macro is known as an operational block, and each daily data directory in the CALIB2 and DERIV2 data sets include a list of the blocks on that day in the BLKLIST.TAB file. In the browse plots, macro numbers are indicated at the start of each block. In the example in **Figure *1*** we find macros 914, 901, 802 and 827.
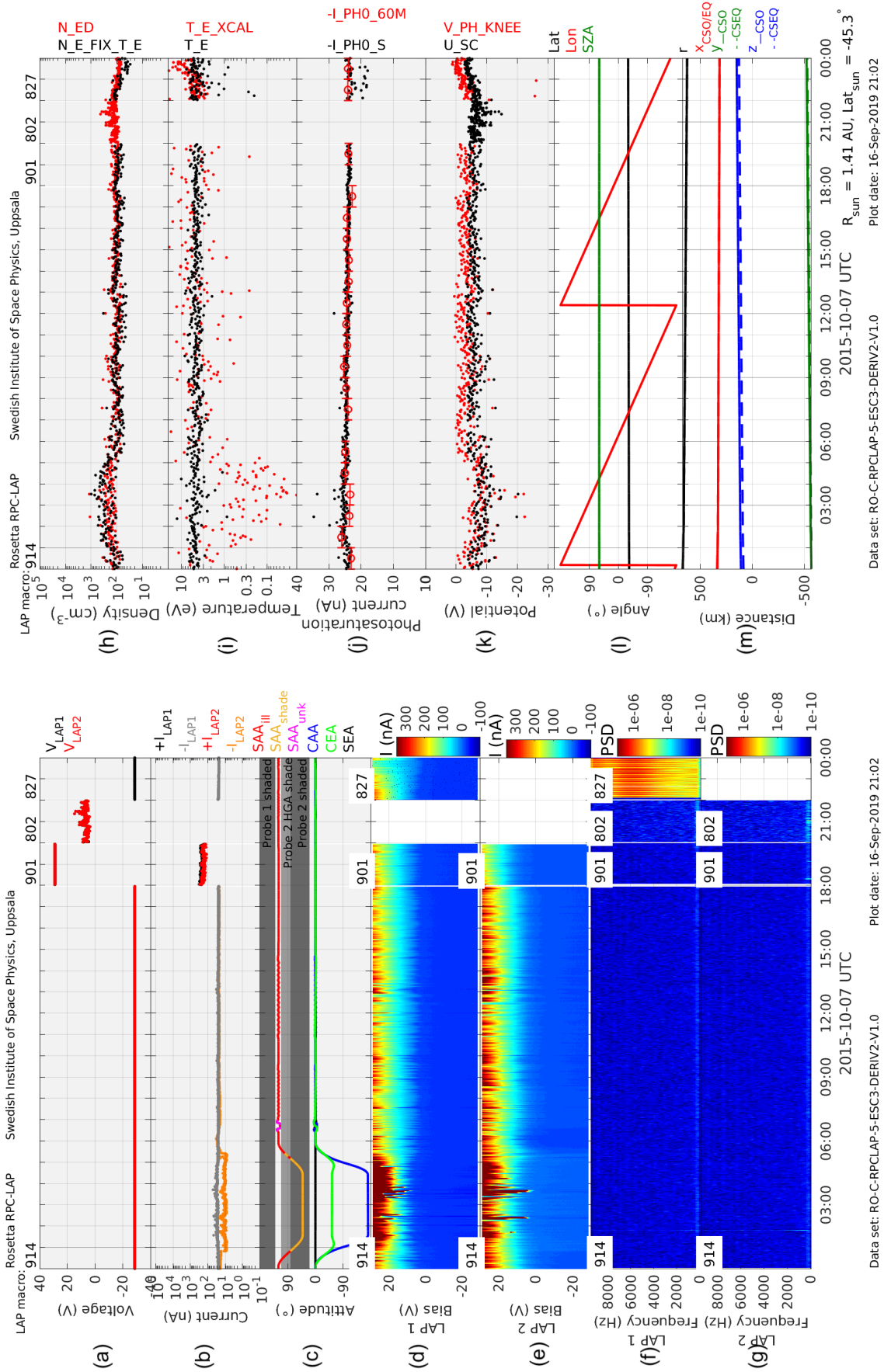
**Figure 1.** Example of a LAP daily browse plot as available in the DERIV2 data sets, except the labels (a)-(m) which have been added here for easy reference in the text.

### 5.1.1 Panel (a): LAP voltages

Quantities plotted: Voltages from I1D, I2D, V1D and V2D files.

There are two principal ways of operating each of the two LAP probes: by applying a bias voltage and measuring the resulting current flowing between probe and plasma (often known as "Langmuir mode"), or by applying a bias current (including zero) and measuring the voltage ("E-field mode"). In **Figure *1***(a), the voltage is plotted, whether it is an applied bias (resulting in a straight line, with data taken from the I1D and I2D files) or a measured value (variable data points, from the V1D and V2D files). It can be seen that bias voltage was applied by all macros run on this day except for the period 20:00-22:00 UTC, when macro 802 runs the instrument in E-field mode. LAP1 is black and LAP2 is red. If both probes give the same value, overplotting will mean only LAP2 is visible. When only LAP1 is visible, as in the last macro block 22:00-midnight, LAP2 is not used. In this case this is because macro 827 hand LAP2 over to the RPC-MIP instrument for its long Debye length mode (LDL).

### 5.1.2 Panel (b): LAP currents

Quantities plotted: Currents from I1D, I2D, V1D and V2D files.

Panel (b) in **Figure *1***(a) shows the currents corresponding to the voltages in panel (a). When the voltage in panel (a) is an applied bias (straight line) the current is a measured value (wiggly line) and vice versa. The vertical scale is linear in early and late mission phases but logarithmic when the comet activity was high and currents very variable. As in panel (a), LAP1 is black and LAP2 red. If the scale is logarithmic and the current negative, the log of its absolute value is plotted and the colours changed to grey and orange, respectively.

### 5.1.3 Panel (c): Spacecraft attitude, probe shading and wake immersion

Quantities plotted: Angles from the GEO files.

Knowing the solar illumination of a Langmuir probe can be important, for example for knowing if the probe is emitting photoelectrons. In interplanetary space, a probe shadowed from sunlight by some spacecraft structure will also be in a solar wind wake. Another type of wake can appear in the flowing cometary plasma. To help assessing such effects, the geometry files in the LAP CALIB2 and DERIV2 data sets provide some useful spacecraft attitude angles.

Panel (b) in **Figure *1*** provides information on the spacecraft pointing with respect to the Sun and the comet nucleus as quantified by four angles. These are conveniently depicted as latitudes and longitudes of the Sun and the nucleus in the spacecraft coordinate system given in **Figure *2*** with the polar axis along +Y and the equator in the ZX plane. Elevation

angle (latitude) is counted positive from the ZX plane toward +Y, while aspect angle (longitude) has its zero meridian along +Z and is counted positive toward +X.
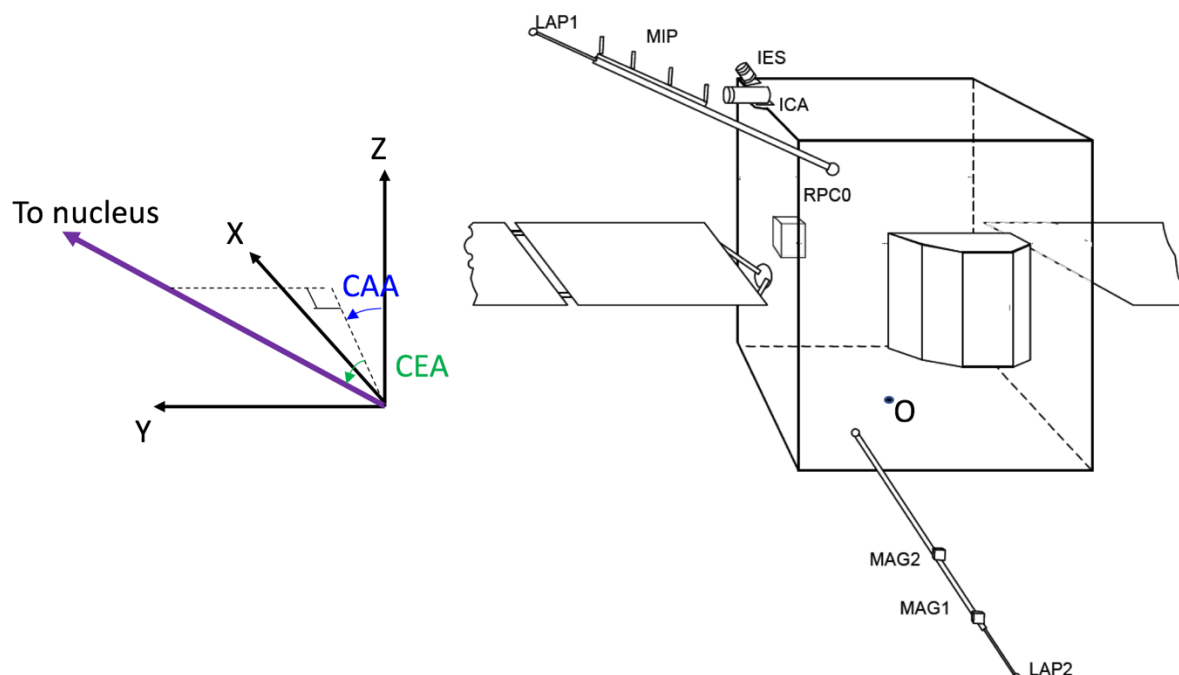


**Figure 2.** The Rosetta spacecraft with the RPC sensors and axes of the spacecraft coordinate system indicated (its origin is at the point O at the centre of the bottom surface in the picture). The comet elevation angle (CEA) and aspect angle (CAA) are indicated, which is the target elevation angle (TEA) and aspect angle (TAA) in the GEO files for the cometary phase data; the corresponding angles for the Sun are similarly defined.

The solar elevation angle (SEA, black) and solar aspect angle (SAA, red/yellow) describe the illumination conditions for surfaces on Rosetta. Nominally SEA = 0 deg, so that the solar panels can always be kept perpendicular to the Sun, though small deviations may sometimes occur, e.g. around 06:40 in **Figure 1**(b). In the nominal SEA = 0 deg case, the s/c +Y axis points perpendicularly to the solar direction, so the illumination of the LAP probes is well defined by the SAA. If this angle is between 131 and 179 deg, LAP1 is in the shadow behind the solar array. This angular interval is the upper shaded region in panel (c), so LAP1 is in shadow when the red curve enters this region; the colour of the curve then is changed to yellow for clearer indication of shadowing. For the same nominal case of zero SAA, sunlight to LAP2 can be blocked by the s/c body, which happens when the SAA enters the lower region of dark shading between 18 and 82 deg in panel (c). However, it may also be shaded by Rosetta's steerable parabolic high gain antenna (HGA) if SAA is in the range indicated by lighter shading (82 to 107 deg). If LAP2 actually is shaded by the HGA cannot be determined from the SAA alone but needs information on the HGA pointing. Such information has been used in the plot, where yellow colour for the SAA curve within the light grey region indicates that LAP really is in the HGA shadow. When shading cannot be properly evaluated because of SEA deviating by more than 1 deg from nominal the curve colour changes to magenta, as is the case around 06:45 in **Figure 1**. The calculated illumination can be directly verified in panel (b), where the two negatively biased probes observe equal current (curves falling on top of each other, so only the LAP1 current is

visible) when both are sunlit, but the LAP2 current can be seen to drop (go less negative) when the probe is in shadow and photoemission thus stops.

In interplanetary space, the direction to the Sun usually does not deviate too much (depending on s/c velocity transverse to that direction) from the direction of arrival of the solar wind. In this case, the conditions for the probe being in shadow and in a solar wind plasma wake are roughly similar, though the latter is much more inexact as the wake does not have a sharp boundary. Nevertheless, SAA and SEA can be used to estimate the risk of such a wake impacting on LAP measurements. At the comet, there is no à priori given direction of the plasma flow, but at least well inside the diamagnetic cavity a radial flow from the nucleus could be expected. For that case, the comet elevation (CEA, green) and aspect (CAA, blue) angles can provide similar indications of the likelihood of a LAP probe being in a wake due to a radial flow from the nucleus as the SEA and SAA does for shadow. In **Figure 1**(c), we can note that after 06:00, CEA $\approx$ 0 deg so CAA can be used to judge wake risk. The blue curve denoting CAA is far (130 deg or more) from the upper shaded area which would indicate a wake problem for LAP1, so we can conclude that LAP1 should be safe from wake effects. On the other hand, CEA $\approx$ 0 deg and therefore LAP2 is just 18 deg away from the boundary of a nominal wake extending straight downstream from the edges of the spacecraft, so if there is a supersonic plasma flow from the nucleus, wake effects on LAP2 cannot be excluded.


## 5.1.4 Panels (d) and (e): Langmuir probe bias sweeps

Quantities plotted: Bias voltages and sweep currents from B1S, B2S, I1S and I2S files in the CALIB2 data set.

The current measured on the LAP probes can be measured while the probe bias voltage is swept (stepped over a number of bias voltage steps). From this fundamental measurement, several plasma parameters can be derived [Eriksson et al., 2017] and are included in the DERIV2 data sets, but for a general impression of the data it can sometimes be useful to look also at the unprocessed current-voltage characteristic available in the CALIB2 data sets. Panel (d) in **Figure 1** displays all LAP1 probe bias sweeps during a day, with the sweep bias voltage on the vertical axis and colour coding for the measured current. Panel (e) shows the same for LAP2. For a macro where any of the probes does not include sweeps the corresponding panel is blank, which in this example plot happens for both probes in macro 802 and for LAP2 in macro 827.

It can be seen from Panel (c) that LAP2 should be in shadow from approximately 00:45 to 05:20. This can be verified directly in Panel (e), as the we find less of negative current at negative bias potentials (corresponding to emission of photoelectrons) on LAP2 during this interval. The big slew away from nominal nucleus pointing the spacecraft is undergoing from the start of the day until about 05:40 obviously has impact on the data, particularly on LAP1.

## 5.1.5 Panels (f) and (g): Power spectra

Quantities plotted: The power spectral density in the PSD files together with the frequency information in the FRQ files.

LAP includes the possibility to sample the currents or voltages it measures up to 18.75 kHz sampling frequency for short snapshots (continuous sampling does not fit within the LAP TM budget). Panel (e) and (f) in **Figure 1** displays spectrograms of such data from LAP1 and LAP2, respectively. The signal from which the spectrum is calculated can be either the probe current (macros 914, 901 and 827 on this day) or voltage (macro 802). The corresponding power spectra are displayed in units of $nA^2$/Hz and $V^2$/Hz, respectively; these units are not indicated in the plots. The signal is detrended by removing a linear least squares fit before calculation of spectra. Interference from RPC-MIP transmission is filtered out (by discarding part of the time series) before Fourier transformation of the waveform data, but when MIP is running in its long Debye length mode (LDL, e.g. in macro 827) some such interference anyway leaks through, as can be seen after 22:00 in this example. When the macro contains no high frequency snapshots, the spectral panel is blank. For macros with reduced sampling frequency (none in this example), the frequency axis is scaled accordingly. The PSD files reside in the DERIV2 data set, while the waveform data from which they are calculated are available in the V1H, V2H, I1H and I2H files in the CALIB2 data sets.

## 5.1.6 Panel (h): Electron density

Quantities plotted: N_ED from the NED files and N_E_FIX_T_E from the ASW files.

Panel (h) in **Figure 1** shows two of the three LAP electron density products available in the L5 data sets, of which one (N_ED) is cross-calibrated with RPC-MIP. The third, N_EL, is (when available) given at much higher time resolution and not suitable for overview plotting. All three are discussed in Section 5.3 below.

## 5.1.7 Panel (i): Electron temperature

Quantities plotted: T_E and T_E_XCAL from the ASW files.

Panel (i) of **Figure 1** shows the two LAP electron temperature products available in the DERIV2 data sets, both of them discussed in Section 5.4 below.

## 5.1.8 Panel (j): Photoelectron saturation current

Quantities plotted: I_PH0_S from the ASW files and I_PH0_60M from the PHO files.

Panel (j) of **Figure 1** shows the two LAP data products giving photoelectron emission current, discussed in Section 5.7. As I_PH0_60M is calculated from all sweeps within one hour, it is here indicated by a ring at the centre of the time slot and a horizontal bar over the

full hour. Note that the value may not necessarily be based on all data from the full one hour interval indicated. The photoemission estimates are further discussed in Section 5.7.

## 5.1.9 Panel (k): Spacecraft potential

Quantities plotted: U_SC from USC files and V_PH_KNEE from ASW files.

In Panel (k) of **Figure 1** are plotted the two LAP data products for the spacecraft potential. Both can be derived from LAP1 sweeps, while macros with LAP1 in electric field mode (macro 802 in the example) will only produce U_SC. The two parameters are further described in Section 5.2.

## 5.1.10 Panel (l): Position angles

Quantities plotted: position angles from the GEO files.

Panel (l) of **Figure 1** shows angles describing the position of Rosetta around the comet nucleus from the 32 s time resolution LAP geometry files. The latitude (black) and longitude (red) are defined in the standard 67P "Cheops" system used throughout the Rosetta project. The latitude changes slowly with s/c motion while the longitude change mostly is due to the nucleus rotation (12-hour period). The Solar Zenith Angle (SZA) is the angle Sun-nucleus-Rosetta, also known as the Phase Angle, so SZA = 0 means Rosetta is on the Sun-Nucleus line. A fourth angle, the latitude of the sub-solar point on the nucleus, is printed at the lower right of each browse plot. This slowly changing angle changes describes the season on the nucleus, being 0 when the comet spin axis is perpendicular to the solar direction. The value given is calculated for noon (12:00 UTC).

## 5.1.11 Panel (m): Position coordinates

Quantities plotted: position coordinates from the GEO files.

Finally, Panel (m) of **Figure 1** shows the Cartesian coordinates of Rosetta in two systems suitable for investigations of the space plasma around in the coma. Target-centred Solar Orbital (TSO) coordinates are the equivalent of Geocentric Solar Ecliptic coordinates at Earth. For the comet phase, the TSO system is known as Cometocentric Solar Orbital (CSO) coordinates: X points to the Sun, Z along the angular momentum vector of 67P's orbit around the Sun, and Y completes right handed coordinate system. The Target-centred Solar Equatorial (TSEQ), and analogously, Cometocentric Solar Equatorial (CSEQ) system has the same X axis as TSO/CSO but its Z axis points along the projection of the angular momentum vector of the solar spin on the plane perpendicular to X: as this is the approximate symmetry axis of the solar magnetic field, at least on long time scales, this system can have some advantages for organizing magnetic observations. In practice, the two systems do not differ much most of the time, as can be seen in the plots. The distance of 67P to the Sun is a slowly changing parameter so a daily value is sufficient: this is printed at lower right in the plot (value applies for noon).

## 5.2 Spacecraft potential

Recommended quantity: U_SC in USC files

For most science purposes, the most useful s/c potential estimate is the U_SC data product in the Level 5 USC.TAB files which is available at 32 to 160 second resolution and covers most of the mission. Depending on instrument operational mode, this is taken either as the negative of the average over 32 s of measured voltage of a sunlit LAP probe (preferably LAP1) floating with no bias current or voltage applied, sometimes known as Vfloat (the averaged data for each probe are available in the V1D and V2D files), or by the equivalent estimate from Langmuir probe bias sweeps, which is the negative of the voltage Vz at which the current to the probe is zero (**Figure 3**). The files include a parameter DATA_SOURCE indicating which of these methods have been used for every single sweep. If the data source listed is Vfloat (either "1" or "2"), there exists higher resolution data down to 16 ms in the Level 3 V1L.TAB or V2L.TAB, which converts to a high time resolution version of U_SC by multiplying with -1.
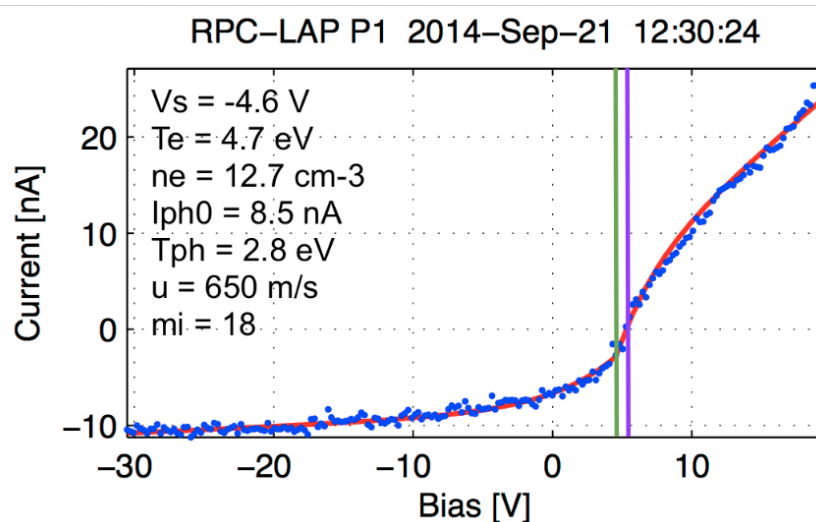


**Figure 3.** Example of a LAP probe bias sweep, with data points in blue and the fit to a model expression with parameters as given indicated by the red curve. The vertical lines in green and magenta indicate V_PH_KNEE and Vz, respectively. For details see Eriksson et al. [2017].

As the U_SC values from Vfloat are averaged they show less variation than Vz, which is an instantaneous and sparse measurement subject to aliasing. In other respects, the data from the two sources are equivalent. We expect U_SC to differ from the true spacecraft potential by a small offset (due to the potential over the probe sheath, of order one volt) and a factor (typically 75-80%) due to some part of the potential field from the spacecraft remaining at the probe position [Odelstad et al., 2016, 2017].

Another potential source of information on the spacecraft potential can be derived from the voltage where the photoelectron emission current from the probe transits from being constant at lower voltages (where all photoelectrons are repelled) to decaying with increasing voltage (as photoelectrons are attracted back to the probe and some of them are reabsorbed) [Eriksson et al., 2017]. This voltage is available as V_PH_KNEE in the ASW files. At high negative s/c potential values, this estimate picks up a slightly lower potential

than Vfloat and Vz but on average provides comparable values. However, as can be understood by looking at the sweep in **Figure 3**, automatic identification of V_PH_KNEE can sometimes be tricky, particular if the electron density is high and (as often is the case) highly variable. In contrast, the zero-crossing defining Vz is relatively simple to identify in **Figure 3**, resulting in data with lower noise level. In addition, Vz and Vfloat should formally be identical, so by using Vz instead of V_PH_KNEE in producing the U_SC estimate we achieve the most consistent dataset covering most of the mission. The only case in which we expect V_PH_KNEE to be a better estimate of Vsc is for positive or only slightly (few volts) negative Vsc values.
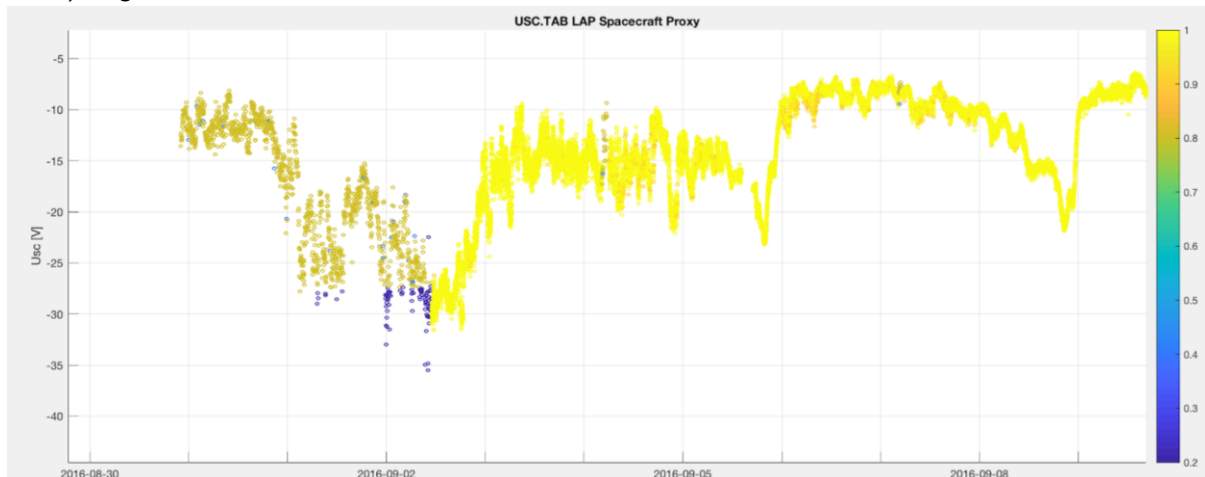


**Figure 4**. Example (covering the period Aug 31 - Sep 9, 2016) of the consistency of the U_SC data set for different sources: Vfloat (yellow), Vz (olive), and extrapolated Vz (blue).

Another advantage of Vz as a Vsc proxy is that it can be extrapolated outside the actual measurement range of LAP. The bias voltage cannot go above +31 V, so if Vsc is near or below -31 V the LAP probes will always be negative with respect to the plasma meaning the current can stay negative in a full probe bias sweep so that no Vz value can be found. However, by cross-calibration with ICA it has been found possible to extrapolate the LAP probe current to find Vz also when outside the nominal range of the instrument.

**Figure 4** shows an example of U_SC data for 10 days in August-September 2016. There is good continuity across mode shifts illustrating that the consistency of the data from both sources of U_SC, and also the extension of the measurement range by Vz extrapolation.

The Vsc estimates can be directly compared in the LAP overview plots (Section 5.1). In **Figure 1**, we can see that U_SC (black) generally falls below V_PH_KNEE (red), particularly when close to zero as expected. It may also be possible to see a slightly higher spread in the V_PH_KNEE estimates than in U_SC. However, it should be noted that the point spread of U_SC mainly is due to actual variations in the plasma, not to any problem with the analysis. **Figure 1** shows that the variations are present in all quantities, including the raw probe bias sweeps. As noted in numerous publications, the comet environment is very dynamic, with the real plasma variations dominating over any measurement noise.

This does not mean that all measurements can be interpreted as real plasma variations. **Figure 1** provides a good example during the period of spacecraft pointing changes, 00:00 - 06:00. The sweeps on LAP1 (Panel(d), see also Section 5.1.4) change character during this

period, so the lower values of both the Vsc estimates in Panel (k) are likely related to the s/c pointing change.

## 5.3 Electron density

Recommended quantity: N_ED in NED files (see also table below)

As discussed in the RPC User Guide, several instruments can provide electron density estimates, many of them in more than one way. In general, MIP provides the best absolute value of the instantaneous electron number density as long as it falls within the range accessible to MIP, LAP has the best time resolution and dynamic range, while the particle instruments ICA and IES mostly detect particles outside the typical energy range of the bulk cometary plasma but are very useful for the low density and high energy solar wind. To combine the good time resolution (and small discretisation steps) of LAP with the accuracy of MIP, cross-calibrated datasets have been derived: the "MIP-LAP" high time resolution data archived with the MIP data and the "LAP-MIP" low time resolution mission wide data set available in the LAP archive as N_ED. There also is the N_EL high time resolution data set, based on LAP data with use of a long-term LAP-MIP cross calibration for some time intervals when MIP-LAP density is not available. Table 1 lists the preferred data sets to be used and some cases for which they may be of interest.

| What is the user interested in? | Which product should the user use? |
|---|---|
| High time (down to 16 ms) total electron density at high absolute accuracy for short periods (~hours) | MIP-LAP electron density in RPCMIP archive |
| High time (down to 16 ms) total electron density at high relative but low absolute accuracy for short periods (~hours) | N_EL in the NEL files in the RPCLAP NEL dataset |
| Electron density at low time resolution for long-term studies (weeks and months) | N_ED in NED files in the RPCLAP DERIV2 dataset |
| High dynamic range total electron density | N_ED |
| Study of a specific day, medium time resolution of the total electron density | MIP-LAP electron density<br>N_ED (LAP-MIP electron density)<br>MIP-only electron density |
| Electron density in the solar wind | N_ED<br>ICA or IES solar wind number density (check both instruments) |

**Table 1**. Various electron density datasets and their potential use.

For a large scale statistical overview over the full mission, the best resource is the LAP data product known as N_ED (N for density, PL for plasma), available in the NED files in the LAP DERIVED2 data sets. The time resolution is most often 160 s. The data here are derived from the LAP Vsc proxy known as U_SC (Section 5.2 above) which is available over all the mission, and are calibrated to MIP density values after 2014-12-31 (Figure 4). Before this period the MIP density detections were scarce since densities usually were low, so here we also use the LAP sweep parameter N_E_FIX_T_E (see next paragraph) for the calibration of U_SC to N_PL. This is a good calibration source precisely when MIP data are scarce, as low electron density means low s/c potential, so the otherwise very negative spacecraft potential here does not prevent plasma electrons from reaching the Langmuir probes.

In principle, errors from different measurement techniques and model assumptions can accumulate, so that the errors in a single cross-calibrated density estimate are potentially larger than in the corresponding MIP source data. However, the MIP discretization is quite coarse due to the finite number of frequency steps available, and the cross-calibrated products perform very well to reduce this discretization down to the much finer LAP resolution.
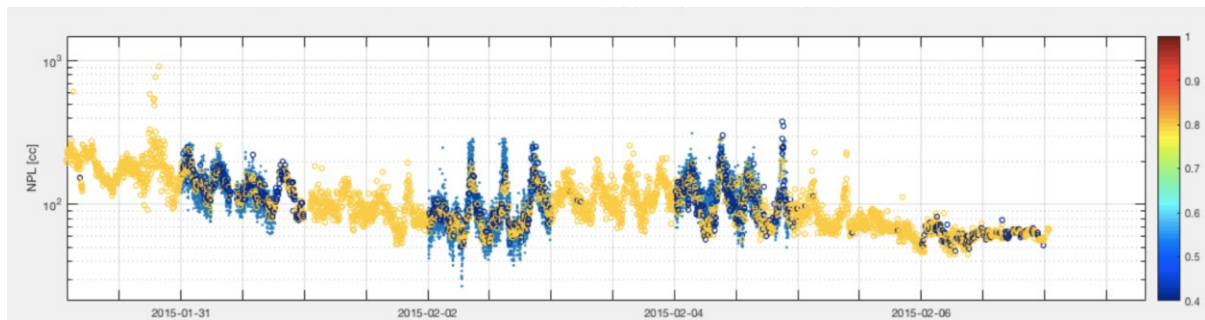


**Figure 5.** Example comparison showing the LAP N_ED electron density colour coded by its quality value and the MIP electron density (in pale blue) for about 9 days. MIP densities are available for three of the days (Jan 31, Feb 2 and 4)  and are used for the calibration of LAP U_SC to the cross-calibrated electron density N_ED over 24 hr windows.

Apart from the N_ED density in the NED files, there is another low time resolution LAP density estimate available as N_E_FIX_T_E in the ASW files. This is calculated from the slope of the probe curve where electron collection dominates (the uppermost few volts in **Figure 3**), which should be proportional to the electron density divided by the square root of the electron temperature [Eriksson et al., 2017]. To follow the trend of the electron density without introducing uncertainties by the large random variations in the LAP electron temperature estimate T_E (Section 5.4), we here assume a fixed electron temperature. We use a value of 5 eV, which has been found suitable for giving densities comparable to MIP at the points where both instruments have data. A user who wishes to use another fixed Te, or or use the sweep-derived T_E, may scale N_E_FIX_T_E by the square root of Te/(5 eV).

While N_E_FIX_T_E works well in low density plasmas, severe underestimation can result in high density plasmas where Vsc becomes very negative. In such situations, the negative Vsc in combination with limited bias voltage range may result in the probe never reaching a potential where electrons are attracted to it, resulting in much too low values of the slope of the probe curve (**Figure 3**, see also discussion in Eriksson et al. [2017]).  Another error, which instead may result in overestimation of the electron density, is the presence of cold

(around or below 0.1 eV) electrons in addition to the warm (few to ten eV) electrons. Due to the inverse square root dependence of the slope on Te, the slope is in such a situation dominated by the cold population, and large errors can result. Note that it does not help to use the T_E estimate (discussed in Section 5.3), as the cold electrons have little impact on the region of the sweep from which T_E it is determined. Using T_E_XCAL (Section 5.4) is formally possible, but as this is determined from the MIP density and the slope, this would only result in retrieving the MIP density value used.

It can be noted that the N_ED electron density product is much less affected by both these errors as it is based on the Vsc proxy U_SC, which by the extrapolation procedure discussed in Section 5.1 covers a wide range of Vsc values, with calibration mainly to MIP density data. This is therefore the preferred standard electron density product, with N_E_FIX_T_E included for comparison and to use when other methods appear to fail.

## 5.4 Electron Temperature

Quantities: T_E and T_E_XCAL in ASW files.

Assuming the electron gas has a Maxwellian distribution of energies, the temperature of the electrons is easiest quantified from the retarding exponential region of the electron current in the LAP I-V curve (around 0 V in **Figure 3**). From LAP as well as MIP data, it is clear that several electron populations often coexist in the coma, typically a warm population around 5-10 eV and a cold one with Te ~ 0.1 eV or lower [Eriksson et al. 2017; Gilet et al. 2017, Engelhardt et al. 2018]. In the ASW files, we therefore provide two estimates of the electron temperature, T_E and T_E_XCAL, where the latter is more influenced by the cold electrons. There are also higher energy populations present as seen by RPC-IES, but these contribute little to the electron bulk density and the LAP Te estimates and are here ignored.

The temperature from the exponential slope of the retarding electron current (a least-square fit slope of the logarithm of the current, after subtraction of a fitted ion current) is provided as the data product T_E in the ASW files, and refers to the warm electron population. If the automatic identification of the retarding electron current region is poor, this estimate can be quite noisy and have a large random spread.
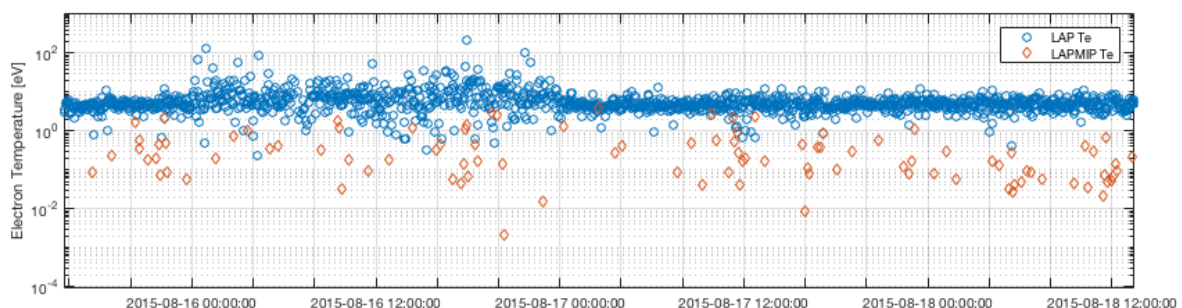


**Figure 5.** The two electron temperature estimates T_E (blue) and T_E_XCAL (red) for three days in August 2015. Cold electrons were only intermittently detected.

As discussed above (Section 5.2) for the N_E_FIX_T_E slope estimate, the slope of the LAP probe curve in the electron attraction region depends on the density divided by the square root of Te, so when cold electrons are present, they can dominate this slope. Engelhardt et al (2018) found that a good indication of the presence of cold electrons is that the slope is larger than 70 nA/V. In such cases, we can therefore combine the observed slope with simultaneous RPC-MIP density estimates to obtain a temperature estimate for the cold population, T_E_XCAL (see Engelhardt et al., 2018, for details). The interpretation should be that when T_E_XCAL has a value below 1 eV, there is a cold electron population present. As the relative fractions of the warm and cold electrons are unknown, the provided value of T_E_XCAL should be interpreted as an upper limit to the temperature of the cold electrons.

It should be noted that the absolute accuracy of the two Te estimates is not well constrained as there is little independent data to compare to. IES temperatures typically refers to a higher energy range, and possibilities for MIP comparison are limited. T_E_XCAL should be seen as an approximate upper value for the cold electron temperature, while T_E should not be considered to estimate the warm electron temperature better than by a factor of two.


## 5.5 Electric Field

Quantity: EFIELD_COMPONENT in EFL files

The two LAP probes could be used to measure the component of the electric field along their separation vector, by measuring the voltage of them, taking the difference and dividing by the separation distance (5.0 m). Each probe could be fed by a bias current as is typically done on electric field instruments in tenuous plasmas, or be disconnected from the bias circuitry to ensure a good zero bias current (floating probes) as is typically done on sounding rockets. Bias currents were used in the early part of the mission, but when the comet ionosphere developed, the floating mode was found to give much more consistent data. Only data from the floating mode have been used for providing E-field data, and only when both probes are sunlit. A data example is displayed in Figure 6.
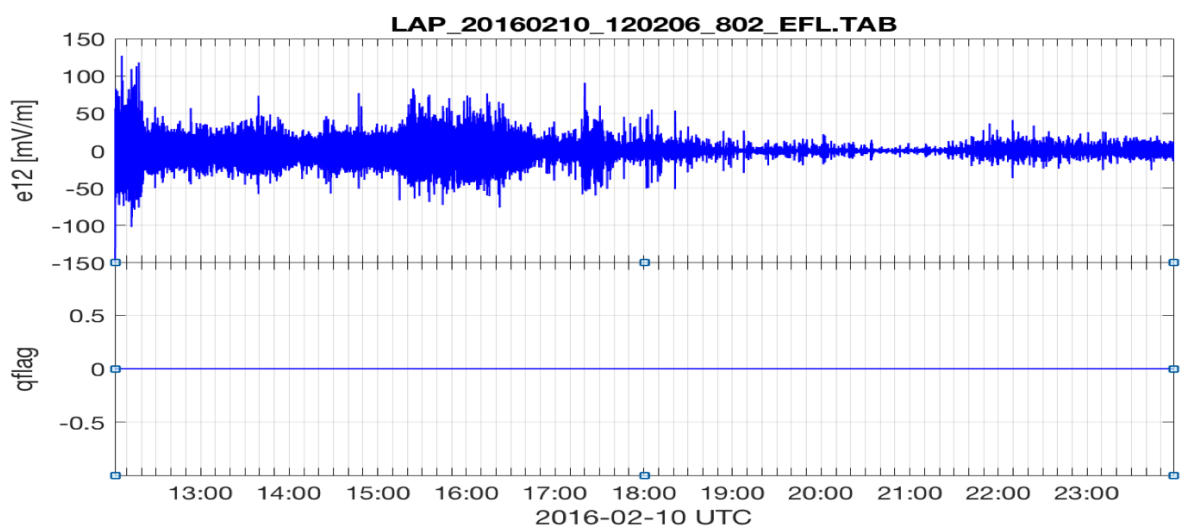


**Figure 6**. Example of LAP E-field data.

The booms are not equal in length (2.24 and 1.62 m) and mounted on a big spacecraft (solar panel wingspan 32 m), so one cannot expect LAP to provide a useful DC electric field estimate. A moving average of the E-field over 32 s is therefore subtracted from the data in the EFL files (for two macros, 0x710 and 0x910, a slightly more complicated procedure had to be used; see [EAICD]). The effective bandwidth of the data therefore is about 0.03 Hz to 20 Hz, the upper limit set by the analog anti-aliasing filters. Note that the filtering may distort the lowest frequencies.

There are no external comparison data for assessing the absolute accuracy of the LAP E-field measurements. The data themselves look very clean and well behaved [Karlsson et al., 2017; André et al, 2017], with very little of common mode signal remaining, despite the s/c potential being both high and highly variable. The technique with floating probes is proven on numerous sounding rockets in the terrestrial ionosphere [Maynard, 1998].

## 5.6 Effective Ion Flow Speed

Quantity: V_ION_EFF_XCAL in ASW files

V_ION_EFF_XCAL is an estimate of the cometary ion effective speed from the ion slope and the RPCMIP density estimates. It is derived from the slope of the LAP I-V curve in the ion saturation region, i.e. the flat region at left in Figure 2. The slope is proportional to density and inversely proportional to ion momentum, so by assuming all ions are $H_3O^+$ (mass 19 amu) and with use of the simultaneous MIP density, it is possible to derive an effective flow speed V_ION_EFF_XCAL. For a plasma with a distribution of ion energies, as should most often be the case, the speed we get is not the arithmetic mean but a harmonic mean (the inverse of the mean of inverses) and so is weighted toward the lowest energies.
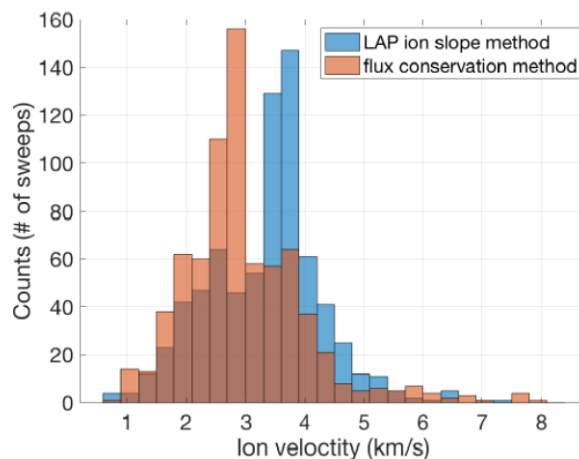


**Figure 7.** Histograms of ion speed estimates in the diamagnetic cavity of comet 67P. The blue values are equivalent to V_ION_EFF_XCAL. [Odelstad, 2018]

Odelstad et al. (2018) compared the speed derived in this way from measurements inside and around the diamagnetic cavity to estimates based on flux conservation and MIP data, finding agreement well within a factor or two (Figure 7). There are no other useful comparison data, as ICA and IES data in the energy range contributing to

V_ION_EFF_XCAL are not well resolved (and much influenced by the usually negative s/c potential) so these data must be treated with caution. A general caveat is that V_ION_EFF_XCAL is useful only in sufficiently dense plasmas and with sufficiently low ion energies. For high energies and/or low density the slope in the probe curve will be very low, and with an instrument resolution of 0.3 nA and temperature dependent offsets not perfectly well known, slopes close to or below 20 pA/V should not be trusted.

## 5.7 Photoemission Current

Recommended quantity: IPH0_60M in PHO files

There are two estimates of the photoemission current from LAP1 sweeps of a sunlit probe. I_PH0_60M in PHO files is a statistical estimate from several sweeps (over 60 minute windows), while I_PHO_S in the ASW files is an estimate from a single sweep with larger uncertainties but higher time resolution (usually 160 s). As LAP1 has shown no significant contamination effects, these estimates should be directly proportional to the EUV flux at the Rosetta position in the 20-130 nm band [Johansson et al, 2017]. For LAP2, the same techniques have revealed a lower photoemission at the start of the cometary phase of the mission, and a sharp drop in photoemission after significant thruster firings (e.g. dayside excursion, 60% decrease) with sporadic recoveries and relapses. We therefore only use LAP1 based values.

While there is no other source of photoemission measurements than LAP, its value is controlled by solar EUV radiation which is known from e.g. TIMED and SDO at Earth and MAVEN at Mars. Photoemission values by both methods were presented by Johansson et al. [2017] and compared to Earth and Mars data. The two methods were found to give consistent results, also in agreement with a third independent method immune to instrument offsets. However, around perihelion all methods returned about 50% less photoemission than expected from the Earth and Mars EUV fluxes. This may be a real effect, for example because of attenuation of solar EUV radiation by large numbers of small dust grains at large distance from the nucleus. It is also possible that this somehow relates to probe surface contamination, though no other such effects have been noted on LAP1.

## 5.8 Wave Activity

Quantity: PSD in PSD files

In addition to quasi-continuous sampling at low frequencies (LF, up to 57.8 Hz), LAP can also sample data at 18,750 samples/s for brief intervals (snapshots). These are known as HF data. The data (currents or voltages depending on the bias mode) are transmitted to ground, possibly after digital filtering and downsampling onboard as time series. These are available in the LAP Level 3 datasets in files identified by the strings I1H, I2H, V1H and V2H depending on sampled quantity and probe. From these data, we calculate power spectra after elimination of parts of each snapshot known to be strongly influenced by MIP interference. The spectra are available as the PSD data product in the PSD files, at 65 frequencies specified in the corresponding FRQ file (Figure 8).
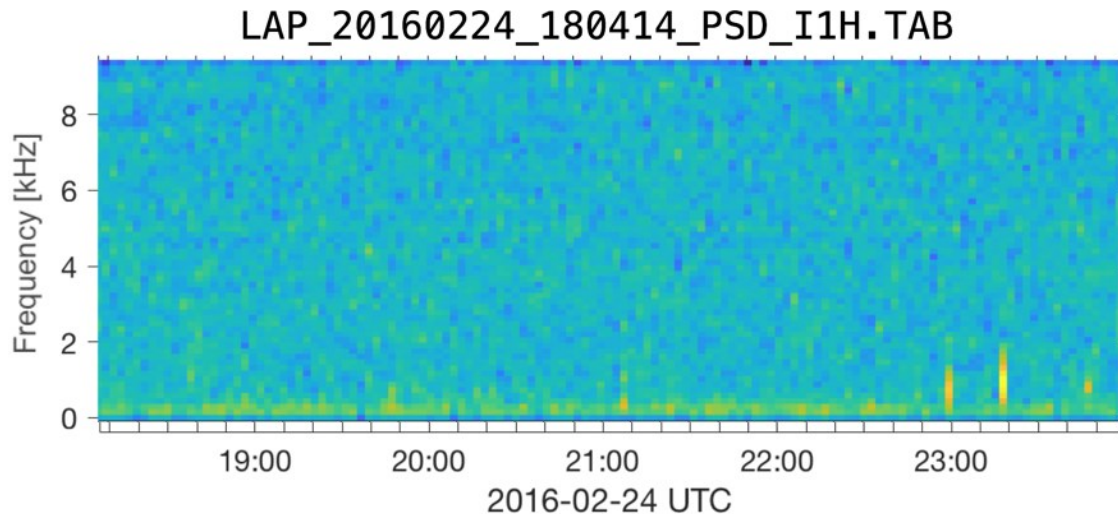
**Figure 8.** Example spectrogram of LAP1 HF data.

While the spectrogram in Figure 8 are calculated from the LAP1 probe current (as seen by the string I1H in the file name), we expect that the signal at these high frequencies is dominated by electric field fluctuations capacitively coupling to the probe. For a discussion of this and other aspects of the LAP HF data, see [Gunell et al., 2017a, 2017b]. Spectral lines at constant frequency should always be treated with suspicion, as likely due to interference. The most limiting aspects of the LAP HF data are the short length of the snapshots (usually a few hundred data points) and the relatively high noise floor in the data as the sampled signal is the same DC coupled probe current or voltage as used for the LF and sweep data.

# 6  Caveats for Level 5 Data

The [EAICD] includes a full list of caveats for the LAP data, including various technical problems. However, many of the issues listed there are not relevant for the L5 data products, as these issues have been treated in the design of the L5 pipeline and selection of L5 data. For example, the problem with the probe current to a positively biased probe sometimes co- and sometimes contravarying with the electron density (due to strong impact of the density on the s/c potential) has been circumvented by not basing any L5 data product on current measurements to a probe at positive fixed bias. Any user analysing L2 or L3 data must consult the EAICD for applicable caveats, but for L5 any important problems and limitations with the data have been discussed in the relevant sections above.

# 7 References

[André et al., 2017] M. André, E. Odelstad, D. B. Graham, A. I. Eriksson, T. Karlsson, G. Stenberg Wieser, E. Vigren, C. Norgren, F. L. Johansson, P. Henri, M. Rubin, I. Richter, Lower Hybrid Waves at Comet 67P/Churyumov-Gerasimenko. *Monthly Notices of the Royal Astronomical Society, 469*, S29-S38, 2017.

[EAICD] ROSETTA RPC-LAP to Planetary Science Archive Interface Control Document, RO-IRFU-LAP-EAICD. Swedish Institute of Space Physics, 2019. (Available in the LAP archive documentation)

[Engelhardt et al, 2018] I. A. D. Engelhardt, A. I. Eriksson, E. Vigren, X. Vallières, M. Rubin, N. Gilet, P. Henri, Cold electrons at comet 67P/Churyumov-Gerasimenko. *Astronomy and Astrophysics, 616*, A51, 2018.

[Eriksson et al., 2017] A. I. Eriksson, I. A. D. Engelhardt, M. André, R. Boström, N. J. T. Edberg, F. L. Johansson, E. Odelstad, E. Vigren, J.-E. Wahlund, P. Henri, J.-P. Lebreton, W. J. Miloch, J. J. P. Paulsson, C. Simon Wedlund, L. Yang, T. Karlsson, R. Jarvinen, T. Broiles, K. Mandt, C. M. Carr, M. Galand, H. Nilsson, C. Norberg, Cold and warm electrons at comet 67P. *Astronomy and Astrophysics, 605,* A14, 2017.

[Gilet et al., 2017] N. Gilet, P. Henri, G. Wattieaux, M. Cilibrasi, C. Béghin, Electrostatic Potential Radiated by a Pulsating Charge in a Two-Electron Temperature Plasma. *Radio Science, 52*, 1432, 2017.

[Gunell et al., 2017a] H. Gunell, H. Nilsson, M. Hamrin, A. Eriksson, E. Odelstad, R. Maggiolo, P. Henri, X. Vallieres, K. Altwegg, C.-Y. Tzou, M. Rubin, K.-H. Glassmeier, G. Stenberg Wieser, C. Simon Wedlund, J. De Keyser, F. Dhooghe, G. Cessateur, A. Gibbons, Ion acoustic waves at comet 67P/Churyumov-Gerasimenko -- Observations and computations. *Astronomy and Astrophysics, 600*, A3, 2017a.

[Gunell et al., 2017b] H. Gunell, C. Goetz, A. Eriksson, H. Nilsson, C. Simon Wedlund, P. Henri, R. Maggiolo, M. Hamrin, J. De Keyser, M. Rubin, G. Stenberg Wieser, G. Cessateur, F. Dhooghe, A. Gibbons, Plasma waves confined to the diamagnetic cavity of comet 67P/Churyumov-Gerasimenko. *Monthly Notices of the Royal Astronomical Society, 469,* S84-S92, 2017b.

[Johansson et al., 2017] F. L. Johansson, E. Odelstad, J. J. P. Paulsson, S. S. Harang, A. I Eriksson, T. Mannel, E. Vigren, N. J. T. Edberg, W. J. Miloch, C. Simon Wedlund, E. Thiemann, F. Eparvier, L. Andersson, Rosetta photoelectron emission and solar ultraviolet flux at comet 67P. *Monthly Notices of the Royal Astronomical Society, 469,* S626-S635, 2017.

[Karlsson et al., 2017] T. Karlsson, A. I. Eriksson, E. Odelstad, M. André, G. Dickeli, K.-H. Glassmeier, A. Kullen, P.-A. Lindqvist, H. Nilsson, I. Richter, Rosetta measurements of lower hybrid frequency range electric field oscillations in the plasma environment of comet 67P. *Geophysical Research Letters, 44*, 2017.

[Maynard, 1998] N. Maynard, Electric field measurements in moderate to high density space plasmas with passive double probes. *Measurement Techniques in Space Plasmas: Fields (AGU Geophysical Monograph 103)*, 13-27, 1998.

[Odelstad et al., 2015] E. Odelstad, A. I. Eriksson, N. J. T. Edberg, F. Johansson, E. Vigren, M. André, C.-Y. Tzou, C. Carr, E. Cupido, Evolution of the plasma environment of comet 67P from spacecraft potential measurements by the Rosetta Langmuir probe instrument. *Geophysical Research Letters, 42* , 10126-10134, 2015.

[Odelstad et al., 2017] E. Odelstad, G. Stenberg Wieser, M. Wieser, A. I Eriksson, H. Nilsson, F. L. Johansson, Measurements of the electrostatic potential of Rosetta at comet 67P. *Monthly Notices of the Royal Astronomical Society, 469*, S568-S581, 2017.

[Odelstad, 2018] Elias Odelstad, *Plasma environment of an intermediately active comet: Evolution and dynamics observed by ESA's Rosetta spacecraft at 67P/Churyumov-Gerasimenko*. PhD thesis, Uppsala University, 2018

[Odelstad et al., 2018] E. Odelstad, A. I. Eriksson, F. L. Johansson, E. Vigren, P. Henri, N. Gilet, K. L. Heritier, X. Vallières, M. Rubin, M. André, Ion velocity and electron temperature inside and around the diamagnetic cavity of comet 67P. *Journal of Geophysical Research, 123*, 5870-5893, 2018.

[RPC User Guide] A. Beth, M. Galand, H. Nilsson, R. Goldstein, P. Mokashi, A. I. Eriksson, F. L. Johansson, I. Richter, C. Goetz, P. Henri, X. Vallières, C. M. Carr, T. Allen, RPC User Guide. (Available in the LAP archive documentation)